Accelerated hygrothermal ageing of bond in FRP-masonry systems

Bahman Ghiassi[1], Paulo B. Lourenço[2], Daniel V. Oliveira[3]

ISISE, University of Minho, Department of Civil Engineering, Guimarães, Portugal

ABSTRACT

This paper addresses the results of accelerated hygrothermal (coupled temperature and moisture) tests on FRP-strengthened clay bricks aimed at investigating bond degradation mechanisms. The exposures are selected to simulate different environmental conditions and the bond degradation is periodically investigated by visual inspection and by conventional single-lap shear bond tests. The changes in the properties of material constituents have also been monitored and the results are presented and critically discussed. A decay model is then adopted for simulating the observed degradation in the specimens. The model, once validated, is used for long-term performance prediction of FRP-masonry systems and the results are compared with the environmental reduction factors proposed by available design guidelines.

Keywords: FRP; masonry; bond; durability; hygrothermal; accelerated ageing.

[1]Postdoctoral Researcher, ISISE, University of Minho, Department of Civil Engineering, Azurém, 4800-058 Guimarães, Portugal. Phone: +351 253 510 499, fax: +351 253 510 217, E-mail: bahmanghiassi@civil.uminho.pt

[2] Professor, ISISE, University of Minho, Department of Civil Engineering, Azurém, 4800-058 Guimarães, Portugal. Phone: +351 253 510 209, fax: +351 253 510 217, E-mail: pbl@civil.uminho.pt

[3]Associate Professor, ISISE, University of Minho, Department of Civil Engineering, Azurém, 4800-058 Guimarães, Portugal. Phone: +351 253 510 247, fax: +351 253 510 217, E-mail: danvco@civil.uminho.pt

Introduction

Modern composite materials such as fiber reinforced polymers (FRPs) have been accepted as effective strengthening materials for civil engineering structures. FRPs provide several advantages comparing to conventional strengthening techniques which have made them interesting for strengthening purposes. FRPs have also received an extensive attention in the last decades for external strengthening of masonry structures (Hollaway 2010).

In external strengthening techniques with composite materials, the efficacy and reliability of the strengthening depends intrinsically on the bond between the composite material and the substrate. The bond behavior has been extensively studied in FRP-concrete systems, but in case of FRP-masonry it has only recently received attention (Grande et al. 2008, Grande et al. 2011, Fedele and Milani 2012, Ghiassi et al. 2012, Valluzzi et al. 2012). However, the durability and long-term performance of bond still remains a challenge for masonry and concrete substrates (Karbhari et al. 2003, Wu et al. 2010). Available information regarding the durability of bond behavior are mostly devoted to FRP-concrete systems under aggressive environments or moisture conditions, see e.g. (Karbhari and Ghosh 2009, Benzarti et al. 2010, Tuakta and Buyukozturk 2011, Marouni et al. 2012, Silva et al. 2013, Kim et al. 2014), and only few researches can be found regarding the FRP-masonry, see e.g. (Sciolti et al. 2012, Ghiassi et al. 2013a, Ghiassi et al. 2013b).

Structures are exposed to environmental changes or degrading agents, such as large temperature and moisture variations or alkaline agents, during their service life. These changes can affect the performance of the structure to a large extent which should be taken into account during the design procedure or should be defeated with innovative solutions. It is thus necessary

to clearly understand the environmental degradation mechanisms and their effects on the structural components or strengthening material.

Most of the environmental factors and deterioration processes are dependent on or coupled with moisture and temperature, and therefore a good understanding of their effects on deterioration of bond is a key step in durability modeling of FRP-strengthened masonry elements. The moisture is known to play an important role in durability of bond in FRP applications, as it reduces the bond strength and fracture energy (Ouyang and Wan 2008, Lau and Buyukozturk 2010, Sciolti et al. 2012, Böer et al. 2013, Ghiassi et al. 2013). The degrading effect of moisture is due to extensive moisture plasticization of the polymer adhesive (which leads to mechanical degradation) and additional breakage of interfacial bonds (Wan et al. 2006). Moreover, the moisture induced vapor and osmotic pressure in the interface can lead to local debonding (Ouyang and Wan 2009). However, the degrading effect of moisture on the bond behavior varies with material properties, surface treatments, and specimens configurations (Sciolti et al. 2012). Temperature cycles below the epoxy glass transition temperature may cause degradation in the bond due to the imposed thermal fatigue and thermal incompatibility between FRP and the substrate (Karbhari et al. 2003). Furthermore, exposure to subzero temperatures and freeze-thaw cycles cause degradation in the bond behavior (Silva et al. 2013). Still, the combined effect of temperature cycles and moisture, the so-called hygrothermal ageing, is not known.

This paper addresses the results of accelerated hygrothermal (coupled temperature and moisture) tests on FRP-strengthened masonry specimens aimed at investigating the bond degradation in these systems. The specimens consist of GFRP-strengthened bricks prepared following the wet lay-up procedure. The bond degradation is assessed by performing conventional single-lap shear bond tests at different periods of exposure. The changes in

mechanical properties of the material constituents are also investigated. The main observations and experimental results are presented and critically discussed. Finally, a decay degradation model is fitted to the experimental results and is used for simulating the long-term behavior of bond in FRP-strengthened masonry.

Experimental program

The experimental program addresses an investigation on the degradation of bond behavior in FRP-strengthened masonry due to hygrothermal conditions. The changes in the material mechanical properties and the bond behavior with exposure time are monitored periodically by performing qualitative and quantitative laboratory tests. The material characterization tests, specimens' preparation, accelerated exposure conditions and post-ageing test methods are presented in this section.

Materials and specimens

Solid clay bricks with dimensions of 200×100×50 mm^3 are used in this study as substrate. The bricks were produced by extrusion without the application of any finishing or glazing on the surface. Glass Fiber Reinforced Polymer (GFRP) is used as the composite material for external strengthening of the bricks. GFRP composites, compared with other conventional FRP materials, have lower axial stiffness that makes them more suitable for masonry structures (Oliveira et al. 2011). The GFRP composites are prepared with a commercially available unidirectional E-glass fiber and a compatible two-part epoxy resin as matrix, following the wet lay-up procedure. A two-part epoxy primer is also used for preparation of the bricks' surfaces before application of FRP composite.

For the material characterization tests, cubic brick specimens, dog-bone shape epoxy and primer specimens and GFRP coupons are prepared according to relevant test standards, see Fig. 1. For the bond characterization, specimens are prepared following the wet lay-up procedure, see Fig. 2. The GFRP sheets with 50 mm width are applied to 150 mm length of the brick's surface leaving a 40 mm unbonded length at the loaded end. The bricks were dried in the oven before application of the GFRP sheets. After cleaning the brick surface, a two-part epoxy primer is applied to the brick's surface. Finally, a two-part epoxy resin is used as the matrix of the composite material and also for adhesion to the masonry substrate.

Mechanical characterization

Mechanical characterization tests are performed according to relevant test standards and the results are presented as the mean value of five tested specimens, see Table 1. The tests are also performed on conditioned specimens for monitoring the changes of mechanical properties of materials with exposure time.

The mechanical properties of bricks are obtained according to standards EN 772-1 (2002) and EN 8942-3 (1986) in terms of compressive strength, f_{cb} and flexural tensile strength, f_{tb}. The compressive strength is obtained by performing compressive tests on 40 mm height brick cubes, in the flatwise direction with a 50 kN Lloyd testing machine, see Fig. 3(a). Three point bending tests are performed on 160×40×40 mm^3 brick prisms to obtain the flexural tensile strength.

Tensile strength and elastic modulus of the epoxy resin and primer are determined from tensile tests on dog-bone shape specimens, see Fig. 1. Although seven days are proposed for curing the epoxy resin in the technical datasheet provided by the manufacturer, the specimens are previously cured for 60 days at room temperature. Previous studies have shown that high curing

times are necessary for complete curing of cold-cured epoxy resins (Frigione et al. 2006, Aiello et al. 2006, Sciolti et al. 2012). The specimens' preparation and tensile tests are conducted following ISO 527-1 (2012). The tests are carried out with an Instron testing machine at a displacement rate of 0.01 mm/min, see Fig. 3(b). Deformation of the specimens is monitored by a clip gauge placed on the middle of the specimens.

The glass transition temperature (T_g) of the epoxy resin is also obtained by means of DSC (Differential Scanning Calorimetry) test. The thermal scans are carried out between 5°C and 200°C with a heating rate of 10°C/min. The T_g is calculated as the mean value of four tests. There are several method of obtaining *T*g commonly used by researchers (Ratna, 2009) (Ratna, 2009) such as Differential Scanning Calorimetry (DSC), Thermo Mechanical Analysis (TMA) and Dynamic Mechanical Analysis (DMA). In DSC, TMA and DMA the specimens are heated through a temperature range to obtain the *T*g. The results obtained from each technique are, usually, different. In reality, the glass transition is a not a specific temperature, but rather a temperature range where several material properties undergo a change. DSC has been widely used by other researchers for durability tests, see e.g. (Sciolti et al. 2012) and is used in this study. It is well known that the values of *T*g depend on several factors such as heating rate and rate of cooling of samples prior to measurements. Therefore, the tests in this study are performed based on the procedure reported in (Mazurin & Gankin, 2007).

Regarding the composite materials, the specimens' preparation and mechanical tests are conducted according to ISO 527-1 (2012). The mechanical properties are obtained in terms of tensile strength, f_{tf}, and elastic modulus, E_f. The tests are carried out with an Instron testing machine at a displacement rate of 0.01 mm/min, see Fig. 3(c). The GFRP coupons are prepared following the wet lay-up procedure according to the code specifications. Throughout this study,

changes in the tensile strength and elastic modulus of GFRP coupons are normalized to the specimens' thickness in accordance with ASTM D7565-10 (2010). In wet lay-up procedures the specimens' thickness varies and the normalization of the mechanical properties by the thickness can provide an accurate baseline for comparison (Cromwell et al. 2011).

As it can be seen in Table 1, the brick presents very low CoVs (about 4%). The GFRP coupons exhibit CoVs about 15%, whereas the epoxy resin and primer exhibit intermediate values, with CoVs about 10%.

Bond characterization

Single-lap shear bond tests are performed to investigate the bond behavior in the reference and aged specimens. The bond tests are performed using a closed-loop servo-controlled testing machine with a maximum load capacity of 50 kN. A rigid steel frame is used to support the specimens appropriately and avoid misalignments in the load application. The specimens are placed on the steel frame and firmly clamped to it as shown in Fig. 4. The tests are driven under displacement control conditions with reference to the LVDT sensor placed at the loaded end of the FRP composite. The specimens are pulled monotonically at a rate of 5μm/sec. The resulting force, F, is measured by means of a load cell. The relative slip between the GFRP and the brick is measured with the LVDTs placed along the bonded length. In general, two LVDTs are glued at the loaded end (denoted by TL and TR), two in the middle of the bonded length (denoted by ML and MR), and one at the free end of the FRP sheet (denoted by B).

Hygrothermal exposure

The specimens are exposed to two different hygrothermal (coupled temperature and moisture) conditions in a climatic chamber. The exposures consisted of 6 hours temperature cycles from +10°C to +50°C and constant relative humidity of 90% (exposure HT1) and 60% (exposure HT2), see Fig. 5. In each cycle, the temperature is kept constant at +10°C for 2 hours, subsequently increased to +50°C in 1 hour, followed by 2 hours constant temperature at +50°C. Then, the temperature is decreased again to +10°C in 1 hour resulting in 6 hours cycles of exposure. The specimens are subjected to a total of 225 cycles of HT1 and 820 cycles of HT2 conditions. The difference in exposure period is due to the fact that the climatic chamber was available for limited periods of time.

As stated in introduction, the available literature on hygrothermal exposure or cyclic temperature exposure conditions on FRP-bonded components is rare and not standardized. Among the few studies found, different exposure conditions are chosen. On the other hand, most of the temperature cycles studies are limited to freeze-thaw conditions and cycle of temperatures in the positive range combined with relative humidity is not common. The temperature cycles used in this study are therefore selected as a reference for further durability tests while considering several factors. The +50°C is relatively a high temperature and is chosen to accelerate the degradation phenomenon, while being far enough from the epoxy resin T_g (70°C). Since environmental conditions can cause reduction (or increment) of T_g in the epoxy resin, the maximum temperature in the thermal cycles should avoid reaching the T_g of the epoxy resin during the tests (Karbhari 2007). It should be noted that measurement of changes in T_g during the tests is critical to understand the state of degradation in the epoxy resin and whether the environmental temperature exceeds this value or not. In this study, the T_g is measured only for the un-conditioned specimens.

Post-ageing tests

Post-ageing tests consist of mechanical characterization and single-lap shear bond tests on the specimens at different exposure periods. The specimens are taken from the climatic chamber and then stabilized in laboratory conditions for four days, before performing the post-ageing tests. Five specimens are tested in each exposure period and the average results are presented next.

The mechanical tests are performed on brick cubes, epoxy specimens and GFRP coupons as explained in sec 2.2. Meanwhile, single-lap shear bond tests are performed to investigate the degradation of bond behavior, as explained in sec. 2.3.

Results and discussion

Material properties

The changes in the compressive strength of bricks due to the hygrothermal exposures are shown in Fig. 6. The change in the bricks compressive strength is negligible in all exposure conditions with a low CoV (maximum 10%). The results show the good resistance of the bricks to the environmental exposures considered in this study.

The changes in mechanical properties of epoxy resin, namely elastic modulus and tensile strength, are presented in Fig. 7 and Fig. 8. A similar degradation is observed in elastic modulus and tensile strength. Some fluctuations can be observed in the test results with exposure time. This can be due to several factors including scatter in the experimental results as a nature of experimental testing, differences in the microstructure and curing of the specimens (although made using the same procedures in a single batch), differences in the porosity of the specimens and variation of the material properties. As these fluctuations are observed between specimens exposed to different exposure periods, the global degradation trend is more important than point-to-point

comparison. While the latter is investigated in the last section of this paper and the graphs are presented together with the predictive decay models, the former is also addressed next at some critical points for performing a local comparison between both exposure conditions. For the elastic modulus, the degradation after 225 cycles is 7%, for both exposures. Meanwhile, for the tensile strength, HT1 induced 20% reduction after 225 cycles of exposure being two times more than the corresponding degradation due to HT2 (10% reduction in both exposures). This difference is clearly due to the moisture attack in exposure HT1 which has resulted in higher degradation in the specimens. The total observed degradation in the epoxy tensile strength is 14% (at 820 cycles) in HT2. 225 cycles is chosen for point-to-point comparison between both exposures at the end of exposure HT1 to avoid extrapolation of the data. The results show that the epoxy resin used in this study has less durability in high humid environments (exposure HT1), although longer cycles of exposure are needed for a clear conclusion. The CoVs of the tests in all exposures are in the range of 2% to 13% which seem reasonable for testing material properties (Haldar and Mahadevan 2000).

The changes in mechanical properties of GFRP coupons together with the scatter of the experimental results are presented in Fig. 9 and Fig. 10. Again, a relatively similar degradation trend is observed in elastic modulus and tensile strength, with exposure HT1 inducing higher degradation in the specimens, as expected. The elastic modulus and tensile strength of the GFRP decreased 23% and 22%, respectively, after 225 cycles of HT1 exposure, with corresponding reductions of 9% and 13% in HT2. The total observed reduction for the elastic modulus and the tensile strength was 22% and 13% in HT2 exposure showing that the degradation in HT2 exposure has reached a residual value. However, reaching a residual value in HT1 cannot be easily concluded at this stage. The CoVs of the experimental results in both exposures are in the

223 range of 5% to 12% which are again typical for testing material properties (Haldar and
224 Mahadevan 2000).

225 The observed degradation can be attributed to different degrading mechanisms. Exposure
226 to temperature cycles, besides the above mentioned effects on the matrix, may cause interfacial
227 micro-cracking due to the difference between thermal expansion coefficients of glass fibers and
228 epoxy resin (Dutta and Hui 1996, Karbhari 2002). The thermal expansion coefficient of E-glass
229 fibers is around 5×10^{-6}/°C, while for the epoxy resin is in the range of $3\sim5\times10^{-5}$/°C (CNR-DT200
230 2004). This one-order magnitude difference of thermal expansion coefficient produces large
231 interfacial thermal stresses at the fiber/epoxy interfaces. In conclusion, the observed degradation
232 in the specimens in HT2 conditions can be a combination of epoxy post-curing, induced thermal
233 fatigue, and the thermal mismatch between epoxy resin and glass fibers. In wet environments
234 (HT1), GFRP coupons absorb moisture which causes degradation in the epoxy resin properties,
235 as described before. Moreover, the water attacks glass fibers resulting in degradation of their
236 mechanical properties and surface energy (Schutte 1994). The fiber/epoxy interface may also
237 degrade due to the degradation of fiber and epoxy resin and also the produced osmotic pressure
238 at the interface (Karbhari 2007).

239

240 **Bond behavior**

241 *Visual inspection*

242 All the specimens are visually inspected periodically, before performing the debonding tests, for
243 investigating the existence of visible interfacial damage or FRP delamination. Although due to
244 the transparency of the epoxy resin, FRP delamination is observable with visual inspection, IR

thermography tests are also performed on specimens for better characterization of delaminations. The results of the IR thermography tests are presented in (Ghiassi et al. 2014).

In general, progressive FRP delamination is observed in the specimens as the exposure cycles increased. The size of delamination is characterized from the IR photos, see Fig. 11(a), with the aim of adopted quantitative IR analysis as explained in (Ghiassi et al. 2014). The delaminations, being at the FRP/brick interface, are generally larger in the specimens subjected to HT1 cycles. The average equivalent debonding length growth with exposure cycles is plotted in Fig. 11(b). The equivalent debonding length is obtained as the debonded area divided by FRP width. This parameter, while providing a clear idea of the debonding progress, is useful for numerical simulations when two-dimensional models are adopted (as is the case for most situations). The specimens exposed to HT2 conditions show a linear debonding growth with a relatively slow rate. However, the debonding growth in the specimens exposed to HT1 conditions is rather large, with an exponential incremental rate.

The observed delamination in the specimens can be attributed to the thermal incompatibility between the composite material and the brick used in this study, as explained before. Additionally, cyclic temperature conditions produce thermal fatigue and may cause FRP delamination from the brick surface during the environmental exposures. The effect of moisture presence on the debonding growth rate is clear in exposure HT1. The moisture attack has resulted in the reduction of surface energy at the FRP-brick interface and therefore the interfacial thermal stresses induced larger delaminations in the specimens exposed to HT1 conditions.

Delamination tests

The changes in the debonding force and slip of the specimens is presented in Fig. 12 and Fig. 13 for both exposure conditions. The debonding force has progressively decreased with the number of exposure cycles. The debonding force decreased 45% and 20% after 225 cycles of HT1 and HT2, respectively. The average reduction of debonding force is 13% at the end of HT2 exposures. Again, it seems that the degradation has reached a residual value. Moreover, the debonding behavior changed from a brittle failure mode to a progressive and less brittle failure mode in exposure HT1. Similar changes in the bond behavior have also been reported in the literature for the specimens exposed to freeze-thaw and wet-dry cycles, see e.g. (Davalos et al. 2008). The higher degradation observed in specimens exposed to HT1 is due to the moisture attack to the interfacial bond between FRP composite and brick and also to the constituent materials. The debonding slip, presented in Fig. 13, is the slip of the GFRP at the moment of debonding obtained from the LVDTs measurements. The debonding slip has been reduced with exposure time in both exposures with a relatively high CoV. It seems that, in HT2 exposure, the reduction of the debonding slip has reached a residual value.

Regarding the failure mode, a progressive change of failure mode from cohesive to adhesive is observed in the specimens after HT1 exposure, see Fig. 14. However, no specific change of failure mode is observed in the specimens exposed to HT2 conditions. Such a change in the failure mode, also reported in (Green et al. 2000), can be attributed to the observed bond degradation during hygrothermal exposure. It seems that the moisture attack has produced a weak line at the FRP-masonry interface (by reducing the interfacial fracture energy) which has resulted in the observed change of failure mode.

A drawback of strength-based approaches in investigating the environmental effects on the bond behavior, as done in Fig. 12, is that the results depend on the geometrical characteristics of the specimens. Fracture mechanics approaches seem to be more appropriate in debonding problems (Tuakta and Buyukozturk 2011). In fracture-based approaches, the degradation parameter is usually the fracture energy or the critical energy release rate. According to CNR DT200 (2004), the bond fracture energy can be obtained from the debonding tests as:

$$G_f = \frac{P_{\max}^2}{b_f^2 (2E_f t_f)} \quad (1)$$

where, $P_{\max}$ is the debonding strength, b_f is the FRP width, E_f is the FRP elastic modulus, and t_f is the FRP thickness. It should be noted that this equation is correct if the bonded length is more than the effective bond length, which is assumed to be the case in this study throughout the whole exposure period. Measurement of the changes in the effective bond length is possible by using strain gauges or through using advanced full field measurement techniques and is not performed in this study. The changes of the bond fracture energy with exposure time are obtained using Eq. (1) and the results are presented in Fig. 15. The results are presented as normalized to the reference fracture energy. The average bond fracture energy value reaches 0.45 N/mm for the reference specimens. The fracture energy has moderate changes due to HT2 conditions (with a 20% reduction at the end of exposure), while a large degradation is observed in the specimens exposed to HT1 conditions (60% total reduction at the end of exposure). It seems that the interfacial fracture energy has reached a residual value in exposure HT2. A comparison between HT1 and HT2 exposures shows that the moisture affects the interfacial fracture energy to a large extent. The interfacial fracture energy in exposure HT1 may have

reached a residual value as well, although performing longer exposure periods is necessary for a clear conclusion.

Assuming that the FRP width and thickness are constant during the hygrothermal exposures, the debonding force is directly related to the square root of interfacial fracture energy and FRP elastic modulus, see Eq. (1). Therefore, the participation of each factor in the degradation of the debonding force can be obtained by plotting the changes in the normalized square root of fracture energy and FRP elastic modulus as shown in Fig. 16. In exposure HT2, the degradation of fracture energy and FRP stiffness has similar effects on the global bond behavior, with the fracture energy having a larger contribution in the bond degradation. The interfacial bond degradation can be attributed to the existing thermal incompatibility inside the composite system and FRP-brick interface. However, when moisture exists in the environment, such as for exposure HT1, the interfacial degradation of the bond has a major effect on the global bond degradation when compared to the FRP elastic modulus. This was expected as moisture is known to cause degradation in the bond strength and fracture energy (Ouyang and Wan 2008, Lau and Buyukozturk 2010, Sciolti et al. 2012, Ghiassi et al. 2013a).

Long-term predictions

This section presents the application of a decay model in predicting the observed degradation in mechanical properties of materials and bond behavior. It should be noted that using predictive models in accelerated ageing tests requires a deep knowledge of the active degradation mechanisms and a large experimental database. The experimental results presented here demonstrated the need for performing longer accelerated ageing tests for exposure HT1 and therefore the predictions made are limited to the available data. Even though, the use of

predictive models assists in better understanding the degradation trends, allows a first comparative study between different exposure conditions and also contributes to development of constitutive models for numerical modeling approaches. Once the decay models are fitted to experimental results, they are used for simulating the long-term performance of the FRP-strengthened elements.

Degradation modeling

An exponential decay model proposed by Phani and Bose (1986) is used next, see Eq. (2). This model has been previously used by other authors for predicting the materials degradation under moisture and temperature conditions, see e.g. (Chen et al. 2006, Nguyen et al. 2012).

$$\sigma_t = \sigma_\infty + (\sigma_0 - \sigma_\infty)\exp(kt) \quad (2)$$

where, σ_t is the strength after exposure to environmental conditions for a period of t, σ_0 is the unconditioned strength, σ_∞ is the residual strength after complete degradation and k is the rate of degradation. Here, the parameters are directly obtained by performing a regression analysis on the experimental data and the results are presented in Fig. 17 to Fig. 18. For the HT2 exposure, the regression analysis is performed for the first 300 cycles so that the accuracy of the model in predicting the degradation until the end of the tests (820 cycles) can be evaluated.

The percent error in the predictions for each exposure is presented in Table 2 and Table 3. Here the f_{te0}, E_{te0}, f_{tf0}, E_{tf0}, P_0 and G_{f0} are the epoxy tensile strength and elastic modulus, GFRP tensile strength and elastic modulus, debonding force and fracture energy of the un-conditioned specimens, respectively. The accuracy of the models is relatively good for all mechanical properties. For the epoxy tensile strength the error range is up to 8.8%, while the error for the elastic modulus is in up to 7.6%. For the GFRP coupons, the error range is up to 4.8% and 10.5%

for the tensile strength and elastic modulus, respectively. Meanwhile, the error in prediction of the debonding force is 18.2% and for the fracture energy is up to 46.4%. The reasonable accuracy of the models in HT2 exposure until the end of the tests, although fitted with 300 cycles of experimental data, shows the suitability of the adopted regression method.

Long-term performance modeling

The proposed predictive models for HT1 and HT2 exposures are respectively used for long-term performance assessment of bond and material properties in environments with high and average relative humidity. As stated before, establishing a link between real exposure conditions and accelerated ageing tests is a complicated task which requires extensive experimental tests. The number of cycles experienced by the materials is considerably influenced by geographic location. Some authors have tried to simulate the real condition of freeze-thaw cycles in different regions assuming each year is equal to 30 to 50 cycles (Barnes 1990, Soudki and Green 1997, Lesko 1999). As an average, it is assumed here that each 40 cycles of hygrothermal exposures represent 1 year life of the structure in real exposure conditions.

Assuming that each 40 cycles represents 1 year of real exposure conditions, the estimations are made for 2000 cycles of HT1 and HT2 exposure for high and average relative humidity environments, respectively. The model reaches a residual value after 50 years (200 cycles), which is the standard code value for structural life expectancy. After 50 years, the degradation in the tensile strength of epoxy resin is 25% and 10% for wet and average humidity environmental conditions, respectively. These values are 7% and 18% for the elastic modulus. For the GFRP, the degradation is 24% and 14% in case of tensile strength, meanwhile it is 26% and 21% for the elastic modulus. For the bond strength 68% and 21% degradation is predicted

for wet and average humidity environmental conditions, respectively. The corresponding predictions for the bond fracture energy are 80% and 25% reductions. The effect of moisture in high relative humidity environments is clear in the predicted degradations.

The lack of knowledge on the long-term performance of FRP-bonded systems has become a major challenge for engineers at the design stage. Some design guidelines, see e.g. (CNR-DT200 2004, ACI 440.7R-10 2010), have recently implemented reduction factors on the material properties for simulating the environmental deterioration effects. According to CNR DT 200 (2004), 25%, 35% and 50% degradation should be assumed in FRP-bonded systems respectively in internal, external and aggressive exposure conditions. The long-term predictions in this study show that the current design methodology may underestimate the degradation factors in wet environments. The degradations for average humidity environments are in good agreement with the CNR DT 200 (2004) reduction factors corresponding to internal/external conditions. However, the predicted degradation in the high relative humidity environment conditions are much higher than the reduction factors proposed in the code for aggressive environments. It is also noted that over factors, such as creep, fatigue or salt crystallization, are not considered but they can have an effect on further reducing the bond strength.

Conclusions

The results of an extensive experimental program aimed at investigating the durability of FRP-masonry systems were presented in this study. Accelerated ageing tests were performed following two different hygrothermal conditions consisting of thermal cycles from +10°C to +50°C with 90% R.H., called HT1, and 60% R.H., called HT2. The HT1 exposure was used for simulating the thermal variations in wet environments, while HT2 simulated environments with

401 average relative humidity. The bond degradation was studied by visual inspection and single-lap
402 shear bond tests. The changes in mechanical properties of material constituents were also
403 investigated. Based on the experimental data, a degradation model was finally used to predict the
404 long-term performance of the studied system. Based on the obtained results, the following
405 conclusions can be drawn:

406 • The hygrothermal exposures did not affect the mechanical properties of the bricks.
407 However, epoxy resin and GFRP coupons showed some degradation. Generally, higher
408 degradation levels were observed due to exposing the specimens to HT1 conditions.

409 • FRP delamination was observed at the FRP/brick interface after exposure to
410 environmental conditions. The delamination, being due to the thermal incompatibility between
411 brick and adhesive, was progressively increased with the number of cycles. Moreover,
412 significantly larger FRP delaminations with higher growth rates were observed in the specimens
413 exposed to HT1 conditions. This can be due to the effect of moisture on the debonding fracture
414 energy and adhesive fracture properties.

415 • A progressive degradation of bond strength and fracture energy was observed in the
416 specimens. The degradation in the specimens exposed to HT2 was very small, contrarily to the
417 large reductions observed in the specimens exposed to HT1 conditions. In HT1 exposure, the
418 failure mode of the specimens changed progressively from cohesive failure in the brick to
419 adhesive failure at the FRP-brick interface due exposure time. However, no significant change of
420 failure mode was observed in the specimens exposed to HT2 conditions.

421 • An exponential predictive model was finally used for modeling the observed degradation
422 in the material properties and bond behavior. The models, once validate, were used for long-term

performance assessment of FRP-strengthened masonry elements and the obtained degradation levels were compared with the reduction factors proposed in the current design guidelines.

Acknowledgements

The first author acknowledges the financial support of the Portuguese Science Foundation (Fundação de Ciência e Tecnologia, FCT), through grant SFRH/BD/80697/2011.

References

ACI 440.7R-10 (2010). "Guide for the design and construction of externally bonded FRP systems for strengthening unreinforced masonry structures", American Concrete Institute.

ASTM D7565-10 (2010). "Standard test method for determining tensile properties of fiber reinforced polymer matrix composites used for strengthening of civil structures".

Barnes, B. A. (1990). "Bond and low cycle fatigue behavior of thermoset composite reinforcing for the concrete industry", M.Sc. thesis , Iowa State University.

Benzarti, K., Chataigner, S., Quiertant, M., Marty, C., Aubagnac, C. (2010). "Accelerated ageing behavior of the adhesive bond between concrete specimens and CFRP overlays", *Constr. Build. Mater.*, 25(2), 523-38.

Böer, P., Holliday, L., Kang, T.H. (2013). "Independent environmental effects on durability of fiber-reinforced polymer wraps in civil applications: A review", *Constr. Build. Mater.*, 48, 360-70.

Chen, Y., Davalos, J.F., Ray, I. (2006). "Durability prediction for GFRP reinforcing bars using short-term data of accelerated ageing tests", *J. Compos. Constr.*, 10(4), 279-86.

CNR-DT 200 (2004). “Guide for the design and construction of externally bonded FRP systems for strengthening existing structures”, National Research Council, Rome, Italy.

Cromwell, J. R., Harries, K.A, Shahrooz, B.M. (2011). “Environmental durability of externally bonded FRP materials intended for repair of concrete structures”, *Constr. Build. Mater.*, 25(5), 2525-39.

Davalos, J.F., Kodkani, S.S., Ray, I., Lin, C. (2008). “Fracture evaluation of GFRP-concrete interfaces for freeze-thaw and wet-dry cycling”, *J. Compos. Mater.*, 42(14), 1439-66.

Dutta, P.K., Hui, D. (1996). “Low-temperature and freeze-thaw durability of thick composites”, *Compos. Part B: Eng.*, 27(3-4), 371-79.

EN 772-1 (2002). “Methods of test for masonry units -Part 1: Determination of compressive strength”.

EN 8942-3 (1986). “Clay bricks and blocks. Test methods”.

Fedele, R., Milani, G. (2012). “Assessment of bonding stresses between FRP sheets and masonry pillars during delamination tests”, *Compos. Part B: Eng.*, 43(4), 1999-2011.

Frigione, M., Aiello, M.A., Naddeo, C. (2006). “Water effects on the bond strength of concrete/concrete adhesive joints”, *Constr. Build. Mater.*, 20(10), 957-70.

Ghiassi, B., Silva, S.M., Oliveira, D.V., Lourenço, P.B., Bragança, L. (2014). “FRP-to-masonry bond durability assessment with infrared thermography method”, *J. Nondestruct. Eval.*, doi:10.1007/s10921-014-0238-8.

Ghiassi, B., Marcari, G., Oliveira, D.V., Lourenço, P.B. (2013a). “Water degrading effects on the bond behavior in FRP-strengthened masonry”, *Compos. Part B: Eng.*, 54, 11-19.

466 Ghiassi, B., Oliveira, D.V., Lourenço, P.B. (2013b). " Experimental investigation on the long-
467 term durability of bond between FRP and masonry substrates", *Proc. FRPRCS11*, Guimaraes,
468 Portugal.
469 Ghiassi, B., Oliveira, D.V., Lourenço, P.B., Marcari, G. (2012). "Numerical study of the role of
470 mortar joints in the bond behavior of FRP-strengthened masonry", *Compos. Part B: Eng.*, 46,
471 21-30.
472 Grande, E., Imbimbo, M., Sacco, E. (2008). "Experimental investigation on the bond behavior of
473 CFRP laminates glued on clay bricks", *Proc. CICE2008*, Zurich, Switzerland.
474 Grande, E., Imbimbo, M., Sacco, E. (2011). "Bond behavior of CFRP laminates glued on clay
475 bricks: Experimental and numerical study", *Compos. Part B:Eng.*, 42(2), 330-40.
476 Green, M.F., Bibsy, L.A., Beaudoin, Y., Labossière, P. (2000). "Effect of freeze-thaw cycles on
477 the bond durability between fiber reinforced polymer plate reinforcement and concrete", *Can. J.*
478 *Civil. Eng.*, 27(5), 949-59.
479 Haldar, A., Mahadevan, S. (2000). "Probability, reliability and statistical methods in engineering
480 design", John Wiley.
481 Hollaway, L.C. (2010). "A review of the present and future utilisation of FRP composites in the
482 civil infrastructure with reference to their important in-service properties", *Constr. Build. Mater*.,
483 24(12), 2419-45.
484 ISO 527-1 (2012). "Plastics-determination of tensile properties- Part 1: general principles".
485 Karbhari, V.M. (2002). "Response of fiber reinforced polymer confined concrete exposed to
486 freeze and freeze-thaw regimes", *J. Compos. Constr.*, 6(1), 35-40.
487 Karbhari, V.M. (2007). "Durability of composites for civil structural applications", CRC Press,
488 Washington.

Karbhari, V.M., Chin, W., Hunston, D., Benmokrane, B., Juska, T., Morgan, R., Lesko, J.J., Sorathia, U., Reynaud, D. (2003). "Durability gap analysis for fiber-reinforced polymer composites in civil infrastructures", *J. Compos. Constr.*, 7(3), 238-47.

Karbhari, V.M., Ghosh, K. (2009). "Comparative durability evaluation of ambient temperature cured externally bonded CFRP and GFRP composite system for repair of bridges", *Compos. Part A*, 40(9), 1353-63.

Kim, Y.J., Siriwardanage, T., Hmidan, A., Seo, J. (2014). "Material characteristics and residual bond properties of organic and inorganic resins for CFRP composites in thermal exposure", *Constr. Build. Mater.*, 50, 631-41.

Lau, D., Buyukozturk, O. (2010). "Fracture characterization of concrete/epoxy interface affected by moisture", *Mech. Mater.*, 42(12), 1031-42.

Lesko, J.J. (1999). "Freeze-thaw durability of polymer matrix composites in infrastructure", *Proc. Duracosys 99*, Brussels, Belgium.

Marouani, S., Curtil, L., Hamelin, P. (2012). "Ageing of carbon/epoxy and carbon/vinylester composites used in the reinforcement and/or the repair of civil engineering structures", *Compos. Part B: Eng.*, 43(4), 2020-30.

Mazurin, O.V., Gankin, Yu.V. (2007). "Glass transition temperature: problems of measurements and analysis of the existing data", *Proc. of International Congress on Glass*, Strasbourg, France.

Nguyen, T., Bai, Y., Zhao, X., Al-Mahaidi, R. (2012). "Durability of steel/CFRP double strap joints exposed to sea water, cyclic temperature and humidity", *Compos. Struct.*, 94(5), 1834-45.

Oliveira, D.V., Basilio, I., Lourenço, P.B. (2011). "Experimental bond behavior of FRP sheets glued on brick masonry", *J. Compos. Constr.*, 15(1), 32-41.

511 Ouyang, Z., Wan, B. (2008). “Experimental and numerical study of water effect on bond fracture
512 energy between FRP and concrete in moist environments”, *J. Reinf. Plast. Compos.*, 27(2), 205-
513 23.
514 Ouyang, Z., Wan, B. (2009). “Nonlinear deterioration model for bond interfacial fracture energy
515 of FRP-concrete joints in moist environments”, *J. Compos. Constr.*, 13(1), 53-63.
516 Phani, K.K., Bose, N.R. (1986). “Hygrothermal ageing of CSM-laminate durign water
517 immersion- an acoustic-ultrasonic study”, *J. Mater. Sci.*, 21, 3633-7.
518 R Ratna, D. (2009). “Handbook of thermoset resins”, iSmithers, UK.
519 Schutte, C.L. (1994). “Environmental durability of glass-fiber composites”, *Mater. Sci. Eng.*,
520 13(7), 265-322.
521 Sciolti, M.S., Aiello, M.A., Frigione, M. (2012). “Influence of water on bond behavior between
522 CFRP sheet and natural calcareous stones”, *Compos. Part B: Eng.*, 43(8), 3239-50.
523 Silva, M.A.G., Biscaia, H.C., Marreiros, R. (2013). “Bond-slip on CFRP/GFRP-to-concrete
524 joints subjected to moisture, salt fog and temperature cycles”, *Compos. Part B: Eng.*, 55, 374-85.
525 Soudki, K.A., Green, M.F. (1997). “Freeze-thaw response of CFRP wrapped concrete”, *ACI*
526 *Conc. Int.*, 19(8), 64-7.
527 Tuakta, C., Buyukozturk, O. (2011). “Deterioration of FRP/concrete bond system under variable
528 moisture conditions quantified by fracture mechanics”, *Compos. Part B: Eng.*, 42(2), 145-54.
529 Valluzzi, M.R., Oliveira, D.V., Caratelli A., et al. (2012). “Round robin test for composite-to-
530 brick shear bond characterization”, *J. Mater. Struct.*, 45, 1761-91.
531 Wan, B., Petrou, M.F., Harries, K.A. (2006). “Effect of the presence of water on the durability of
532 bond between CFRP and concrete”, *J. Reinf. Plast. Compos.*, 25(8), 875-90.

533 Wu, Z., Kim, Y.J., Diab, H., Wang, X. (2010). “Recent developments in long-term performance
534 of FRP composites and FRP-concrete interface”, *Adv. Struct. Eng.*, 13(5), 891-904.
535

List of Tables

List of Figures

566 Table 1. Material properties (five specimens).

Clay brick		Average	CoV(%)
Compressive strength	f_{cb} (MPa)	14.3	4.0
Flexural tensile strength	f_{tb} (MPa)	1.5	24.6
Epoxy resin			
Tensile strength	f_{te} (MPa)	53.8	9.7
Elastic modulus	E_{te} (GPa)	2.5	9.5
Ultimate strain	ε (%)	2.6	10.4
Primer			
Tensile strength	f_{tp} (MPa)	55.3	11.1
Elastic modulus	E_{tp} (GPa)	2.9	6.1
Ultimate strain	ε (%)	2.1	14.5
GFRP coupon			
Tensile strength	f_{tf} (MPa)	1250	15.0
Elastic modulus	E_{tf} (GPa)	79.2	6.8
Ultimate strain	ε (%)	1.9	20.2

567

568

569

570 Table 2. Error in degradation modeling in HT1 exposure.

Cycles	Epoxy				GFRP				Bond			
	f_{te}/f_{te0}	Err. (%)	E_{te}/E_{te0}	Err. (%)	f_{tf}/f_{tf0}	Err. (%)	E_{tf}/E_{tf0}	Err. (%)	P/P_0	Err. (%)	G_f/G_{f0}	Err. (%)
0	0.99	-1.1	1.00	-0.1	1.00	-0.2	0.99	-0.5	1.08	7.6	1.00	-0.3
60	0.95	5.4	0.97	0.2	0.89	4.1	0.82	-1.1	0.87	-10.1	0.82	-17.7
120	0.91	-4.4	0.96	0.9	0.83	-3.9	0.76	3.0	0.73	-11.9	0.69	-25.6
180	0.89	-6.2	0.95	-1.8	0.80	3.3	0.75	1.7	0.63	18.2	0.58	46.4
225	0.87	8.8	0.94	1.0	0.79	0.8	0.74	-3.9	0.58	5.4	0.51	30.0
Average Err.		5.2		0.8		2.5		2.1		10.6		24.0

571

572

573

574 Table 3. Error in degradation modeling in HT2 exposure.

Cycles	Epoxy				GFRP				Bond			
	f_{te}/f_{te0}	Err. (%)	E_{te}/E_{te0}	Err. (%)	f_{tf}/f_{tf0}	Err. (%)	E_{tf}/E_{tf0}	Err. (%)	P/P_0	Err. (%)	G_f/G_{f0}	Err. (%)
0	1.00	-0.1	1.00	-0.1	1.01	0.9	1.00	-0.1	1.02	1.8	1.05	4.8
120	0.93	0.4	0.94	2.6	0.93	-4.8	0.92	-4.0	0.89	-10.1	0.89	-13.4
180	0.91	-5.4	0.92	-7.6	0.90	1.8	0.89	10.5	0.86	2.3	0.85	-2.8
250	0.91	3.7	0.90	4.6	0.88	1.7	0.87	-4.1	0.83	4.9	0.81	17.1
360	0.90	3.2	0.88	6.7	0.87	-2.2	0.84	-4.5	0.81	-12.8	0.79	-19.8
480	0.90	-2.5	0.87	5.7	0.86	2.7	0.82	3.3	0.80	6.2	0.77	8.5
600	0.90	-0.8	0.86	5.8	0.85	4.5	0.81	2.1	0.79	-5.9	0.77	-14.7
710	0.90	-1.9	0.86	0.0	0.85	-2.9	0.80	-6.0	0.79	-3.7	0.76	-3.7
820	0.90	-0.9	0.85	0.7	0.85	-4.7	0.80	1.7	0.79	-9.2	0.76	-21.2
Average Err.		2.1		3.7		2.9		4.0		6.4		11.8

575

576

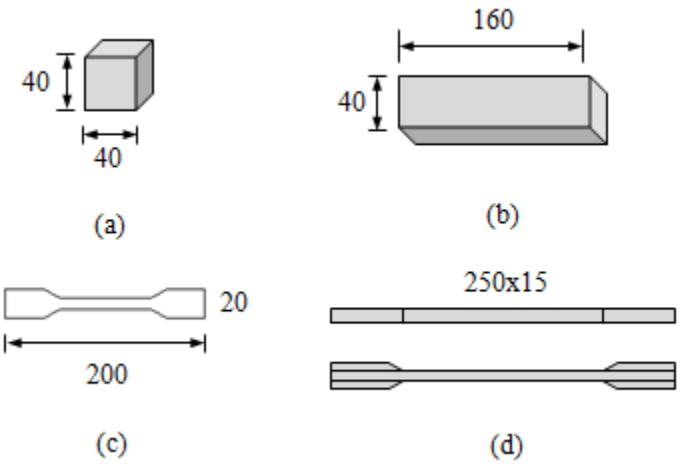

Fig. 1. Specimens used for material testing (dimensions in mm): (a) brick cubic specimen; (b) brick prism; (c) epoxy resin and primer; (d) GFRP coupon.

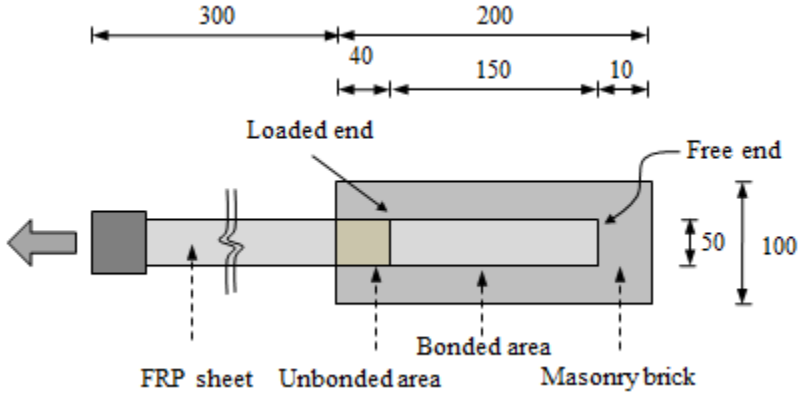

Fig. 2. Geometry of specimens prepared for bond tests (dimensions in mm).

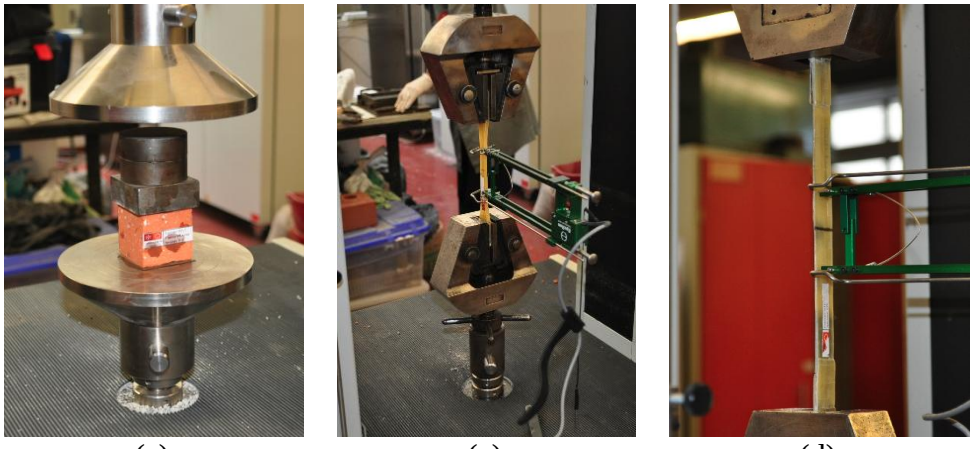

(a) (c) (d)

Fig. 3. Mechanical characterization test setups: (a) brick compressive test; (b) epoxy tensile test; (c) GFRP tensile test.

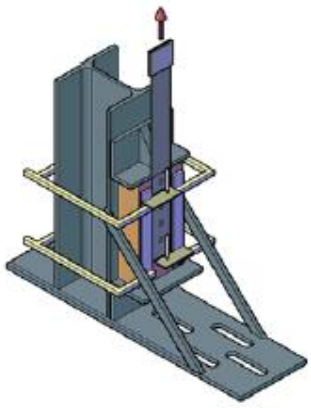

586 Fig. 4. Single-lap shear bond test setup (perspective).

587

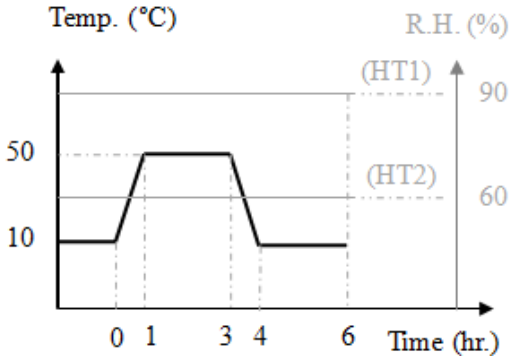

588
589 Fig. 5. Hygrothermal exposures.
590

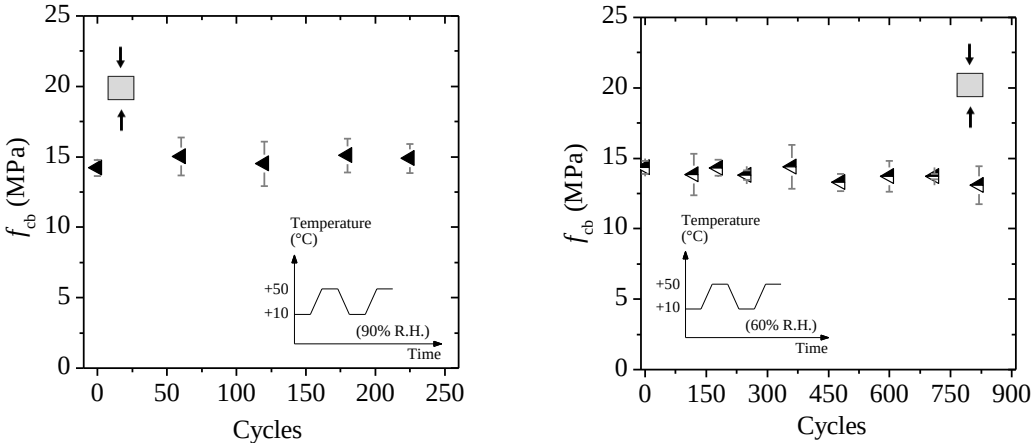

591 Fig. 6. Degradation of bricks compressive strength due to exposures: (a) HT1; (b) HT2.
592

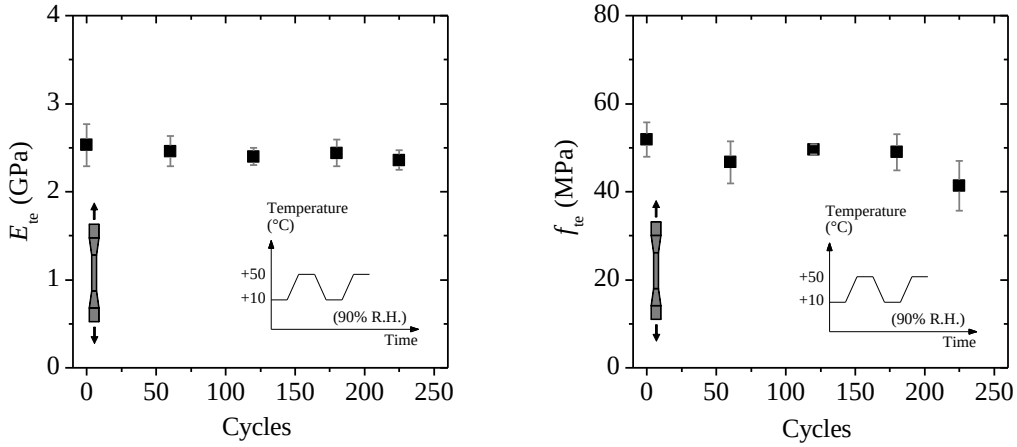

(a) (b)

593 Fig. 7. Effect of exposure HT1 on epoxy resin: (a) elastic modulus; (b) tensile strength.

594

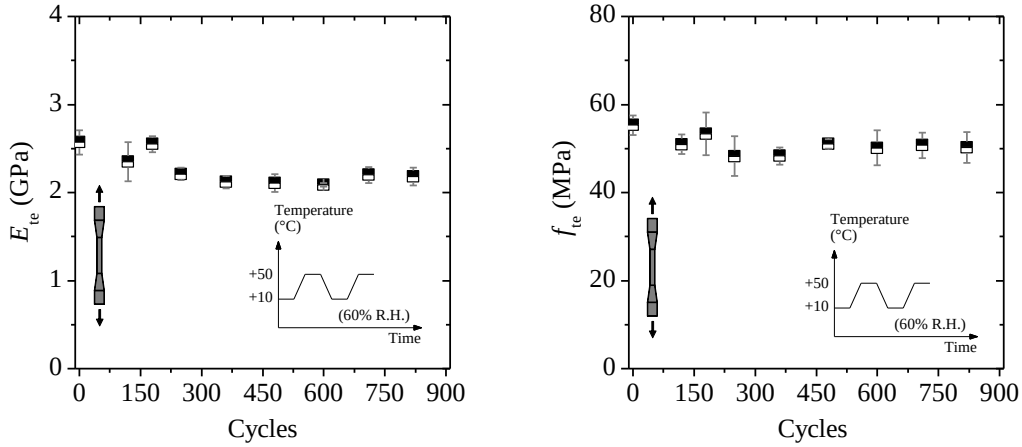

(a) (b)

595 Fig. 8. Effect of exposure HT2 on epoxy resin: (a) elastic modulus; (b) tensile strength.

596

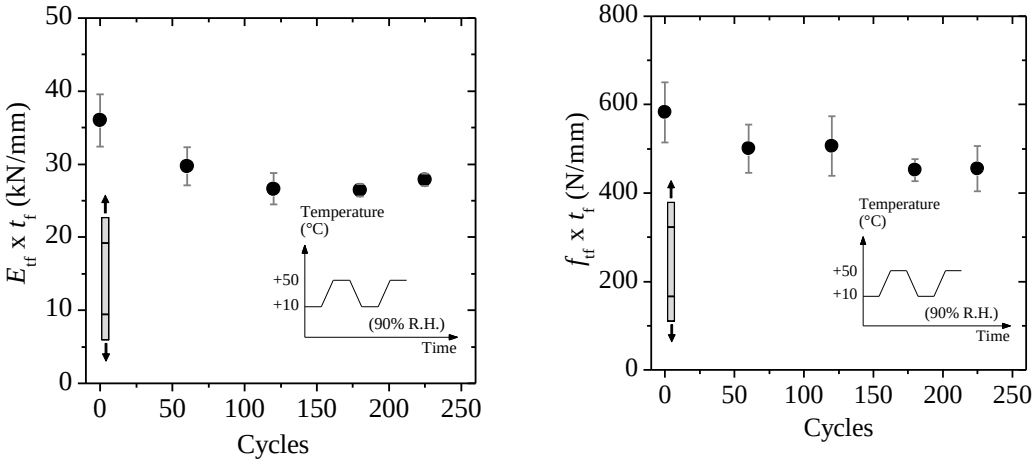

(a) (b)

597 Fig. 9. Effect of HT1 exposure on GFRP coupons: (a) elastic modulus; (b) tensile strength.

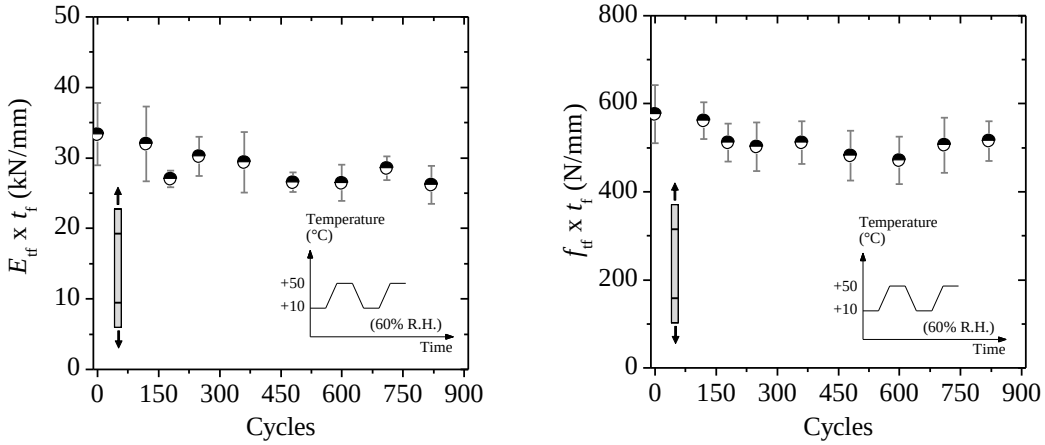

(a) (b)

598 Fig. 10. Effect of HT2 exposure on GFRP coupons: (a) elastic modulus; (b) tensile strength.
599

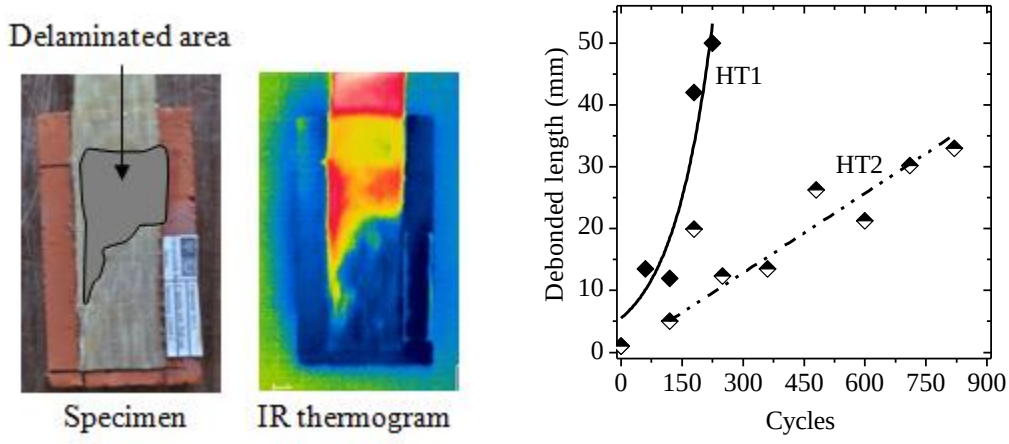

(a) (b)

600 Fig. 11. Hygrothermal induced delaminations: (a) IR thermography results; (b) debonded length
601 growth.
602

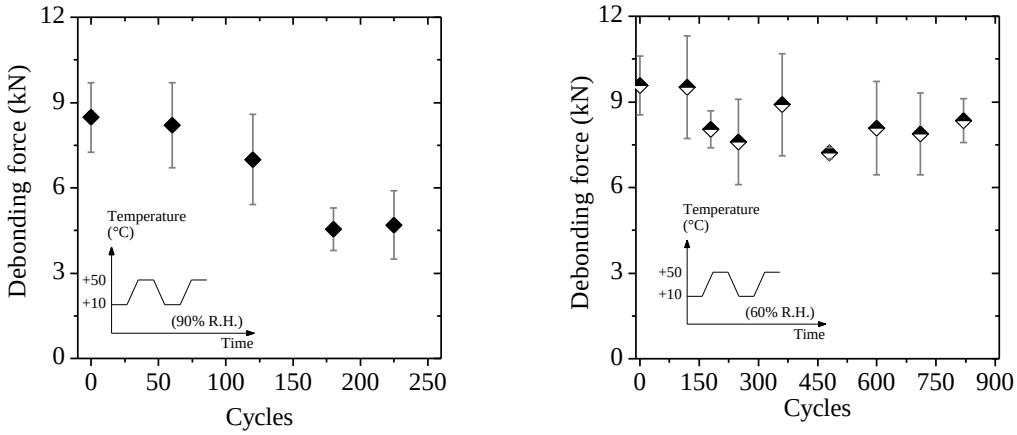

(a) (b)

603 Fig. 12. Debonding force degradation due to exposure: (a) HT1; (b) HT2.

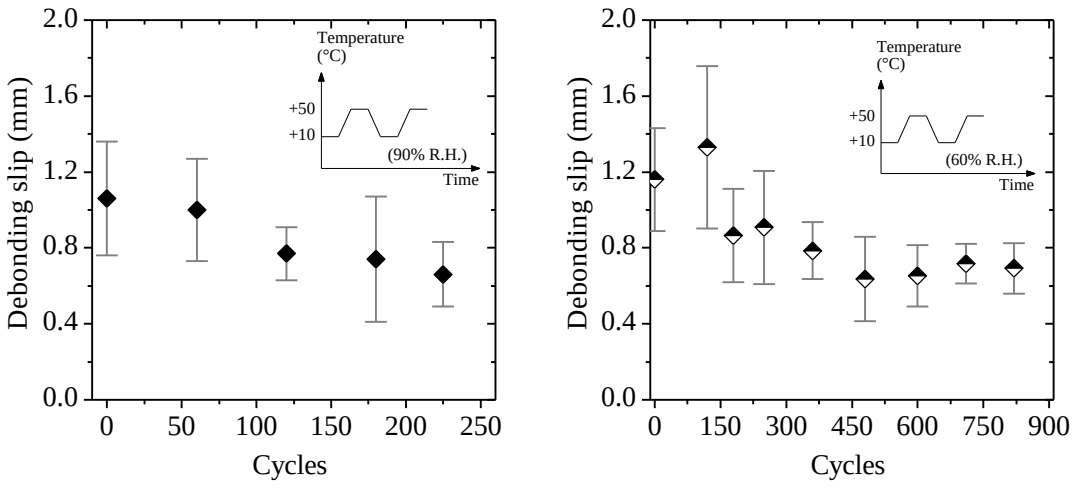

Fig. 13. Changes in debonding slip due to exposure: (a) HT1; (b) HT2.

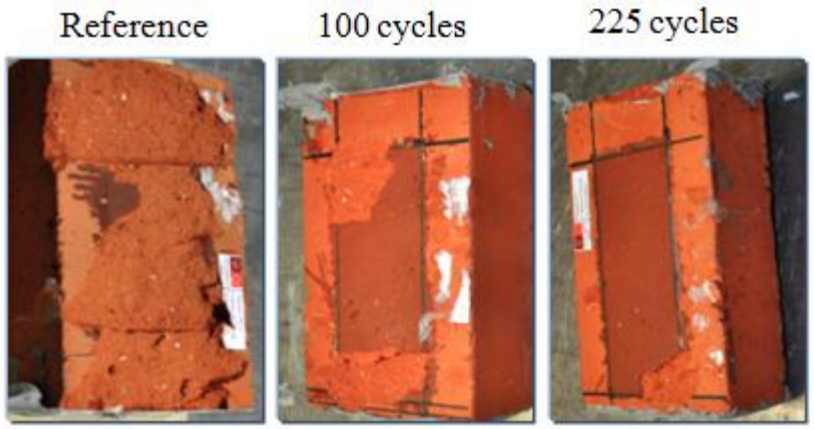

Fig. 14. Change of failure mode in the specimens during HT1 exposure.

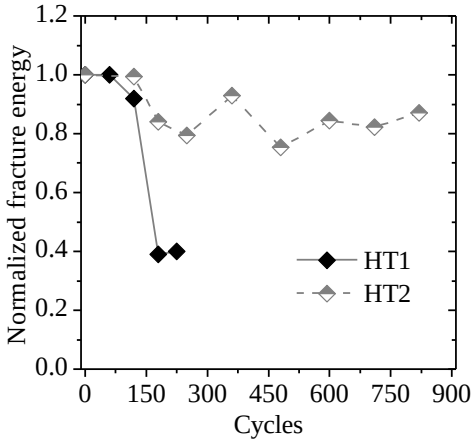

609

610 Fig. 15. Degradation in the fracture energy.

611

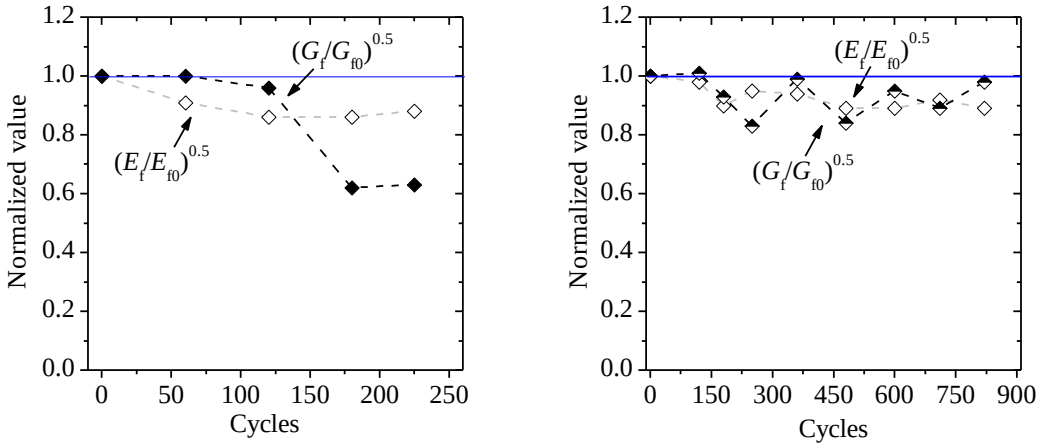

(a) (b)

612 Fig. 16. Bond degradation mechanisms in: (a) exposure HT1; (b) exposure HT2.

613

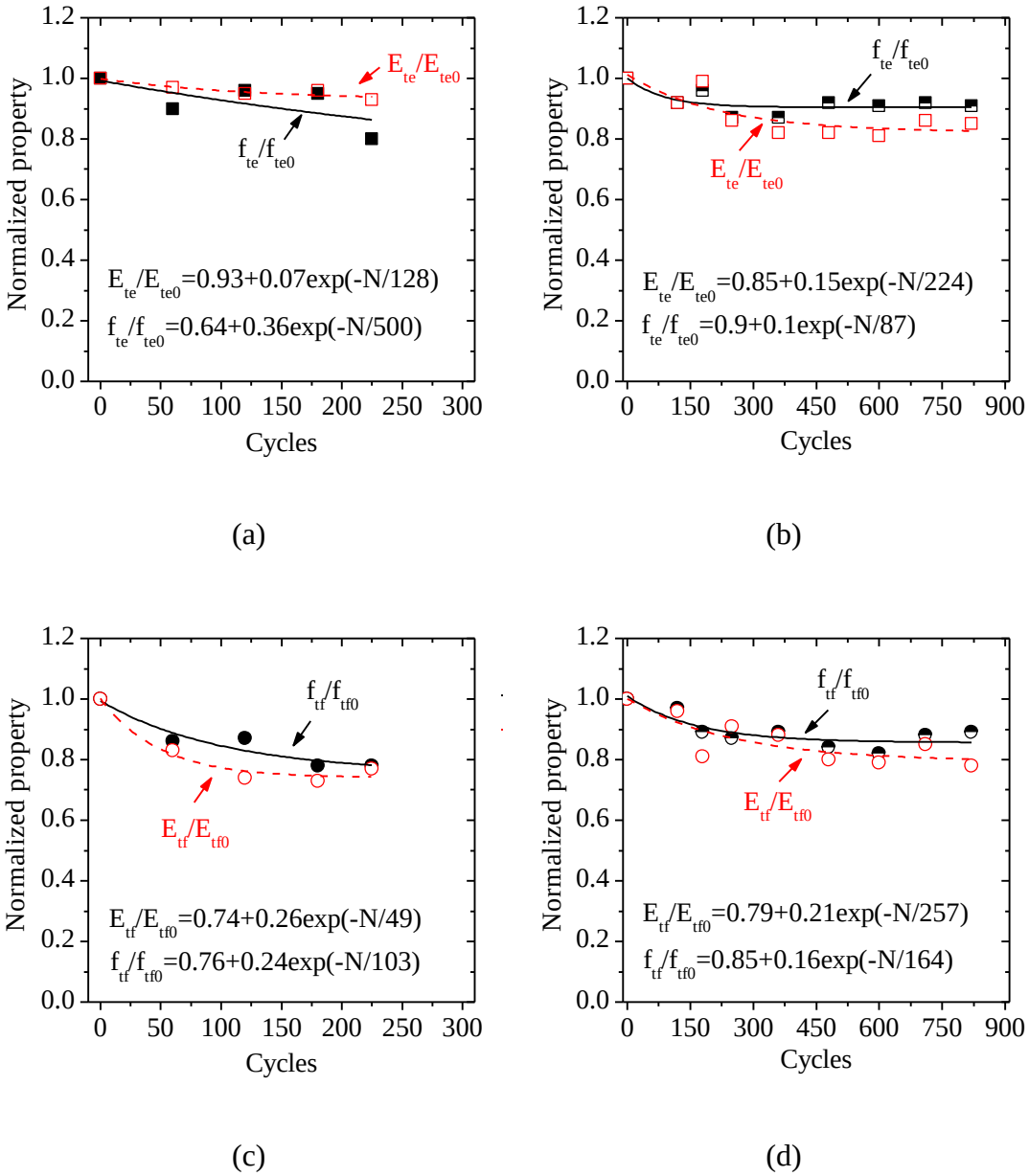

Fig. 17. Modeling the degradation in: (a) epoxy resin in HT1 environment; (b) epoxy resin in HT2 environment; (c) GFRP in HT1 environment; (d) GFRP in HT2 environment.

618

619

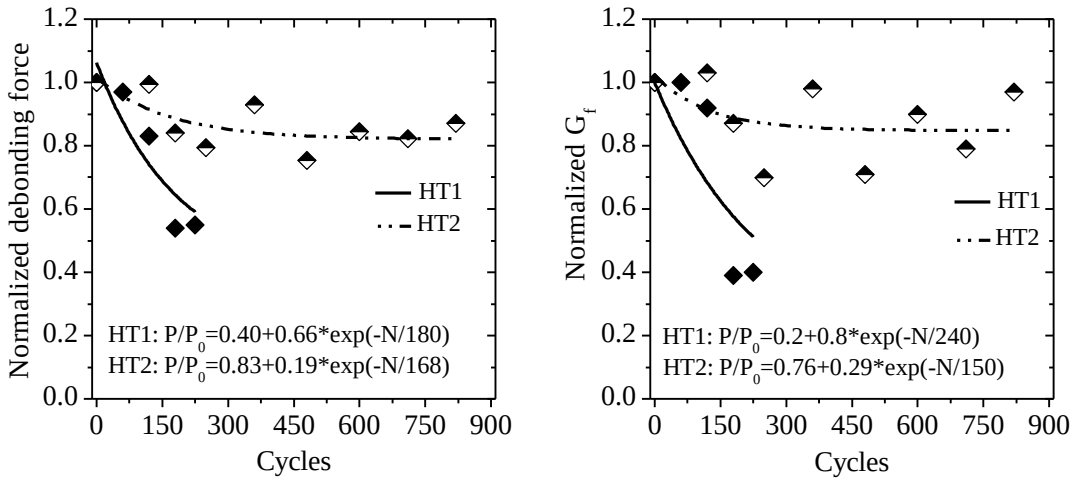

(a) (b)

620 Fig. 18. Modeling the degradation of bond: (a) debonding force; (b) fracture energy.

621